Energy Reports 8 (2022) 13824–13836

Contents lists available at ScienceDirect

Energy Reports

journal homepage: www.elsevier.com/locate/egyr

Research paper

Research on variable speed constant frequency energy generation based on deep learning for disordered ocean current energy

Hongbo Wei *, Wenbin Su, Junxiao Shi

School of Mechanical Engineering, Xi'an Jiaotong University, Xi'an 710049, Shaanxi, China

ARTICLE INFO

Article history:
Received 29 July 2022
Received in revised form 9 September 2022
Accepted 11 October 2022
Available online xxxx

Keywords:
Deep learning
Energy conversion
Variable speed and constant frequency
Ocean current energy

ABSTRACT

As one of the most promising new energy sources today, ocean current energy has become an important part of energy strategies. There are short-term disorderly fluctuations in the flow rate of ocean current energy. The uncontrolled input of kinetic energy from the ocean current can lead to poor quality of power generated by current energy generators. The existing technology of current energy generation uses mechanical rigid transmission, which is prone to fatigue damage and low reliability under variable load fluctuations. In this paper, a joint simulation platform based on AMESim and Simulink is constructed based on 50kW hydraulic transmission and control power generation equipment. This paper establishes a mathematical model of the hydraulic transmission control system and proposes a constant frequency control algorithm based on a deep learning prediction model to improve the steady-state accuracy of the hydraulic motor speed. This paper proposes a deep learning prediction model based on EWT (Empirical Wavelet Transform)-LSTM (Long Short-Term Memory)-CNN(Convolutional Neural Network), which improves the prediction accuracy by 12.26% compared to short-term memory neural network. The model improves the motor speed dynamic accuracy by 90%, the standard deviation index by 78.11%, and the maximum deviation by 86.10% compared to the feed-forward Proportional Integral Derivative (PID)control algorithm. Therefore, the model can effectively improve the quality of the system's power generation. At the same time, the time cost of the model for a single prediction is less than the sampling time of other control algorithms. In this paper, the simulation results are verified by a 50kW hydraulic transmission control experimental bench. The constant frequency control algorithm based on the deep learning prediction model can effectively improve the constant frequency dynamic accuracy of the motor of the hydraulic transmission control power generation equipment, which in turn improves the system power generation quality.

1. Introduction

In recent years, the world's economy has grown at a rapid pace with the continuous advancement of technology. The demand for energy has also become stronger in various countries (Wang et al., 2021; Li et al., 2022b,a). In the International Energy Agency (IEA) reference example, renewable energy sources are anticipated to generate roughly 29.2 percent of the world's net power in 2040, making them the source of electricity with the quickest rate of growth (Qadir et al., 2021). As a result, researchers around the world are striving to find alternative sources of clean, renewable energy (Nasr Esfahani et al., 2022; Zhang et al., 2022).

Ocean current energy is an important form of ocean energy. The energy density of ocean current energy is high, about four times that of wind energy and 30 times that of solar energy (Kim et al., 2012; Djama Dirieh et al., 2022).

There is some fluctuation in the flow rate of ocean current energy, which generally varies in a disorderly manner. Many researchers have made predictions about the energy of ocean currents. Liu et al. proposed a deep learning model based on weighted pure attention mechanism for ocean current with the first attempt to use the weighted pure attention mechanism to improve the ocean current prediction performance (Liu et al., 2022). Using a simulation experiment for an observation system, Jacobs et al. illustrate that the separation of confined and unconstrained characteristic scales is governed by time–space observation coverage (Jacobs et al., 2021).

The principle of current energy generation is similar to that of wind power, and al-most any wind turbine can be converted into a current energy generator (Nachtane et al., 2020a). Similar to how wind energy uses local tidal currents, ocean current energy does the same, as shown in Fig. 1 (Nachtane et al., 2020b). The kinetic energy of flowing water is captured with this method using ocean current energy converters like ocean currents turbines. The turbine dynamic model was created by Jiang et al. using the Blade

* Corresponding author.
E-mail address: whb1427@stu.xjtu.edu.cn (H. Wei).

https://doi.org/10.1016/j.egyr.2022.10.300

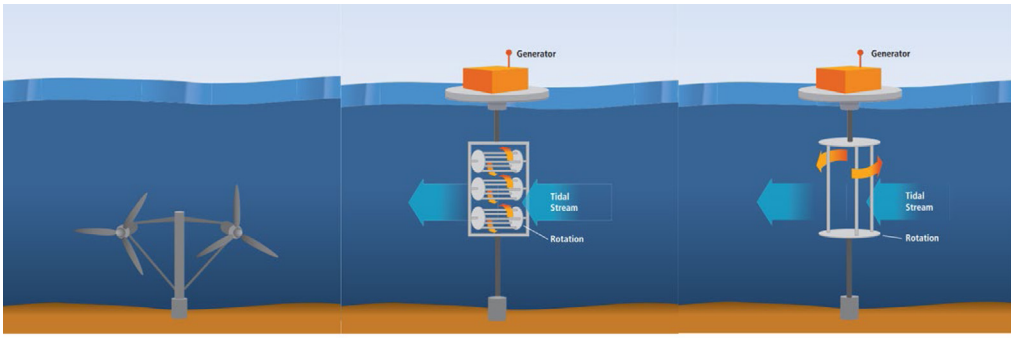

Fig. 1. Ocean current energy converters. (a) twin turbine horizontal axis device. (b) cross-flow device. (c) vertical axis device. (design by National Renewable Energy Laboratory).

Element Momentum (BEM) theory and Bernoulli's principle. They also resolve the form parameters of the turbine blades using the nonlinear optimization approach, and trial production of the light arc and NACA airfoil blades at low flow rates follows Jiang et al. (2021). Utilizing a rotor model customized to the Moroccan potential and the Blade Element Momentum, Hazim et al. performed a thorough analysis of the hydrodynamic stresses of a three-blade horizontal-axis marine turbine. For a turbine, they computed the hydrodynamic stresses, estimated the energy performance, and chose the ideal blade specifications. Hazim et al. (2020). In summary, current energy turbines are currently the main method of capturing current energy, but the speed of current energy turbines is influenced by the flow rate of current energy.

Ocean current energy may be complicated by turbulence. As a result, there may also be considerable short-term variations in current speed, which are disordered and cannot be accurately predicted. Generators traditionally require high-speed unidirectional drives, which may be constant or variable speed. Zhang et al. examined the impact of ocean current turbines powered by Doubly Fed Induction Generators (DFIG) on a distribution network when the grid's voltage is imbalanced. According to their research, DFIG ocean current turbines can deliver effective damping, and modern DFIG ocean current power plants with power electronics and low-voltage ride-through capability can maintain connections to weak electrical grids even in the presence of unbalanced voltage conditions without compromising system stability (Zhang et al., 2017). In summary, the short-term disorderly variation of the current energy flow rate leads to the disorderly variation of the turbine speed, which in turn affects the energy conversion and power generation quality of the current energy. The current technical research has not yet achieved stable control of turbine speed under disorderly changes in current energy.

Hydraulic transmission and control power generation systems are widely used in the field of wind power generation and ocean current energy generation. The use of hydraulic transmission for the conversion of ocean current energy, replacing the traditional gearbox, has the advantages of stepless speed regulation, absorption of load fluctuations and flexible connections, which can improve the reliability of the system.

Variable frequency pump-controlled motor speed control system using single neuron adaptive PID control has faster response characteristics and good dynamic characteristics. Variable frequency pump-controlled motor speed control systems have a good dynamic response to the system flow output using a compound control method with load feedforward compensated PID feedback. Conventional control algorithms are in practice due to the existence of linear drift in the proportional amplifier and the poor repeatability accuracy, resulting in the actual output value of the traditional algorithm constantly changing, leading to large feed-forward errors at different hydraulic pump speeds. However, deep learning has been less studied in relation to quantitative pump-variable motor speed control systems.

In response to the above problems, this paper studies and analyzes a deep learning control algorithm-based hydraulic drive control power generation system for ocean cur-rent energy, which is suitable for low current energy generation systems with disorderly variations. This hydraulic drive control system uses a volume pump-variable motor as a stepless speed control system. A constant frequency control algorithm based on a deep learning prediction model is developed in this paper. The paper analyzes the mathematical model of the hydraulic transmission and control power generation system and uses the deep learning prediction model to predict the effect of changes in ocean current flow rate on the motor speed. This paper improves the constant-frequency dynamic accuracy by correcting the feed-forward control amount through a compensation controller. A combined EWT-LSTM-CNN deep learning prediction model is investigated in this paper, with an accuracy improvement of 12.26% compared to the LSTM neural network. The paper verifies the simulation results based on a 50 Kw experimental bench, and the algorithm is effective in improving the constant frequency accuracy of the power generation unit and hence the quality of power generation.

2. Theory and method

This paper focuses on the analysis of an ocean current energy generation system, which simulates disordered ocean current energy by means of a frequency converter, as shown in Fig. 2. In this paper, the hydraulic system part of the power generation system is accurately controlled based on deep learning algorithms, which in turn enables the dynamic accuracy control of the hydraulic motor speed. To investigate the dynamic performance of the system, this paper designs a constant frequency control algorithm to achieve a constant motor speed to improve the quality of the power generation. The following mathematical model of the hydraulic transmission and control system is developed for simulation and analysis in this paper.

2.1. Mathematical models for hydraulic systems

Firstly, it is assumed that there is no pressure drop in the oil circuit and that the parameters in each line are consistent. Secondly, it is assumed that there are no leaks throughout the hydraulic system and that the effect of the charging system is ignored. Finally, it is assumed that the oil is incompressible and

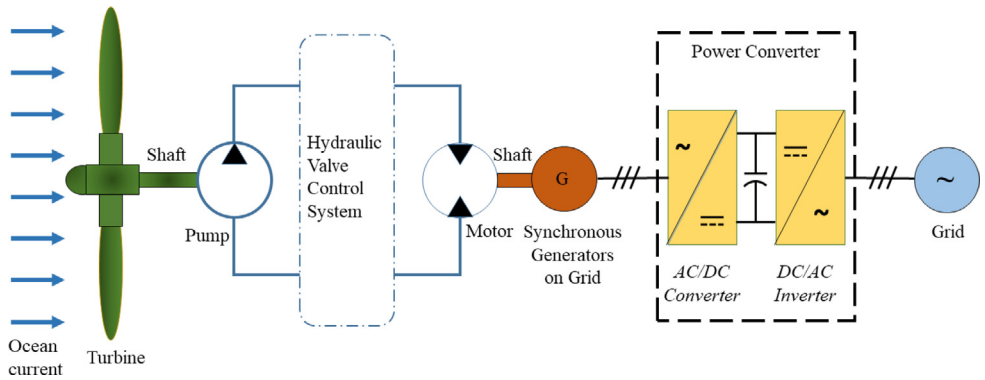

Fig. 2. Flow chart of hydraulic power generation system for ocean current energy (Su et al., 2021).

the density is consistent. Based on the above assumptions, this paper establishes the following transfer function.

The speed of the quantitative pump is changed by the speed of the motor, at the same time, its displacement remains the same, the mathematical model of the quantitative pump can be expressed as follows.

$$Q_p = V_p n_p - C_{tp} P_h \tag{1}$$

where Q_p is the flow rates for fixed displacement pump, V_p is the displacement of fixed volume pump, n_p is the speed of the fixed displacement pump, C_{tp} is the internal leakage coefficient of fixed displacement pump, P_h is the pressure of the high-pressure tube of the fixed displacement pump.

The mathematical model of a variable displacement motor can be expressed as follows.

$$Q_m = V_m n_m - C_{tm} P_h \tag{2}$$

where Q_m is the variable motor flow, V_m is the displacement of variable motor, n_m is the speed of variable displacement motor, C_{tm} is the internal leakage coefficient of variable displacement motor.

The mathematical model of the hydraulic system piping can be expressed as follows:

$$Q_p - Q_m = \frac{V_0 dP_s}{B_e dt} \tag{3}$$

where Q_p is the flow rates for fixed displacement pump, V_o is the volume of the line between pump and motor B_e is the bulk modulus of elasticity of hydraulic oil.

The mathematical model of the coupled fixed displacement pump, variable motor, and hydraulic system piping yields.

$$V_p n_p - V_m n_m = \frac{V_0 dP_s}{B_e dt} + (C_{tp} - C_{tm}) P_s \tag{4}$$

The transform is applied to the equation.

$$V_p \Delta n_p - V_m \Delta n_m = (\frac{V_0}{B_e} s + C_{tp} - C_{tm}) \Delta P_s \tag{5}$$

At the same time, the balance equation for the variable motor torque is as follows.

$$V_m P_s = T + J_m \frac{dn_m}{dt} + B_m n_m \tag{6}$$

The Laplace transform is applied to the equation.

$$V_m \Delta P_s = \Delta T + 2\pi J_m s \Delta n_m + 2\pi B_m \Delta n_m \tag{7}$$

Combining the two equations gives the following transfer function between motor speed, motor displacement and pump speed.

$$\Delta n_m = \frac{\frac{V_m V_p \Delta n_p}{V_m^2} - \frac{C_t}{V_m^2}(1 + \frac{V_0}{C_t B_e} s)\Delta T}{\frac{JV_0}{B_e V_m^2} s^2 + (\frac{JC_t}{V_m^2} + \frac{B_m V_0}{B_e V_m^2}) s + 1} \tag{8}$$

The load torque balance equation for a variable motor is as follows:

$$V_m P_h = T + 2\pi J_m \frac{dn_m}{dt} + 2\pi B_m n_m \tag{9}$$

where T is the external load torque acting on the variable motor shaft, J_m is the rotational inertia of variable motors, B_m is the viscous damping coefficient.

2.2. Deep learning predictive models

The feed-forward control volume in the above hydraulic transmission and control power generation equipment is analyzed. This paper ignores the volume and leakage of the pipeline between the dosing pump and the variable motor and considers the internal leakage coefficient of the pump and the variable motor as 0. Then the mathematical model of the hydraulic system can be expressed as:

$$\omega_t V_p = \omega_m V_m \tag{10}$$

Therefore, the feed-forward control amount can be set as follows:

$$V_m = \frac{\omega_t V_p}{\omega_m} \tag{11}$$

However, in the actual system, when the change in ocean current flow rate causes the pump speed to change, the transfer function of the system regarding the pump speed is as follows, with higher order differential links and inertia links. The rigidity of the overall system is influenced by the frequency of the change in speed, where parameters such as the internal leakage coefficient of the dosing pump and variable motor and the volume in the pipeline all have an effect on the dynamic accuracy of the pump speed.

$$\frac{\Delta n_m}{\Delta T} = \frac{-\frac{C_t}{V_m^2}(1 + \frac{V_0}{C_t B_e} s)}{\frac{s^2}{\omega_h^2} + \frac{2\zeta}{\omega_h} s + 1} \tag{12}$$

According to the above analysis, based on the above mathematical model of the hydraulic transmission and control power generation system, the traditional control algorithm feedforward PID algorithm whose constant frequency control dynamic accuracy does not reach the ideal value. The reason for this is mainly due to the unreasonable setting of the feed-forward control amount. In order to solve this problem, this topic uses a constant-frequency control algorithm based on a deep learning prediction model to provide a correction value for the feedforward control quantity. By predicting the future motor speed at time k based on the deep learning prediction model, the feedforward control amount is corrected by comparing it with the target

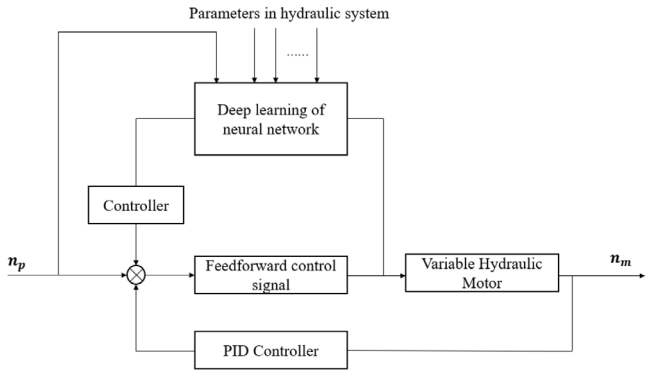

Fig. 3. Block diagram of a constant frequency control algorithm based on a deep learning predictive model.

value of the motor speed via the controller. This paper focuses on deep learning algorithms through LSTM, CNN and EWT, and the above three algorithms will be studied in detail in subsequent chapters. In addition, Back-Propagation Neural Network (BPNN) and Deep Belief Network (DBN) algorithms are also commonly used deep learning algorithms. Due to BPNN's superior non-linear mapping, generalization, and self-learning capabilities, it has been shown that it is frequently utilized in the field of engineering optimization. The BPNN training period is overly long due to an abundance of training data. It just uses one cluster to train the BPNN model and treats the clustering's center as the label. Therefore, accurate information might be lost in other clusters. The DBN is a deep neural network that has numerous layers of hidden cells. It may also be thought of as a graphical model that is stacked with different Restricted Boltzmann Machines (RBMs). The control algorithm schematic and block diagram are shown in Fig. 3.

The design of the compensating controller for the feed-forward control quantity, where deviations in pump speed still exist under feed-forward control, is as follows.

$$\Delta\omega = \omega_m^{predict} - \omega_m \tag{13}$$

where is ω_m the set values and $\omega_m^{predict}$ is the predicted value.

Expanding the above equation can be written as:

$$\Delta\omega = \frac{V_p\omega_p}{V_m + V_m^T} - \frac{V_p\omega_p}{V_m} \tag{14}$$

$$V_m^T = -\frac{\Delta\omega V_m^2}{V_p\omega_p + \Delta\omega V_m} \tag{15}$$

where V_m^T is the compensated motor displacement.

The control signal converted to variable motor displacement is as follows.

$$s = -\frac{c_{max} - c_{min}}{V_m^{max}} \times (V_m - \frac{\Delta\omega V_m^2}{V_p\omega_p + \Delta\omega V_m}) + c_{max} \tag{16}$$

2.3. Basic idea of the EWT-LSTM-CNN algorithm

In this paper, the LSTM algorithm is used as the basis of the model. To overcome the shortcoming that the LSM model parameters cannot extract features at scales other than the time scale, the CNN is used to optimize the influence factor feature selection of the LSTM model and to construct an EWT-LSTM-CNN based model for predicting the sea current flow rate. The algorithm uses CNN neural networks for feature extraction of the influence factors of the data. At the same time, the EWT algorithm is used to extract the different modal information in the load data to maximize the retention of feature information in the current velocity series, thus improving the accuracy of the prediction model. The flow chart of the EWT-LSTM-CNN prediction algorithm is shown in Fig. 4. The specific steps are described as follows.

(1) Firstly, the ocean current velocity data is pre-processed, including missing data processing, text data quantization processing, and data normalization processing.

(2) The CNN network is used to convolve the load sequences containing the influence factors to extract the features of the influence factors and obtain the local correlation between the current velocity data.

(3) EWT is used to decompose the current velocity prediction to obtain the modal feature information of the current velocity data at different scales.

(4) The component LSTM prediction model is established by forming the corresponding input matrices from the influence factor feature series and each modal component.

(5) The prediction structure of each component LSTM model is reconstructed to obtain the final EWT-LSTM-CNN prediction results.

3. Research on constant frequency control algorithm based on deep learning prediction model

3.1. Predictive model based on LSTM

LSTM networks are a special type of RNN and are commonly used in time series prediction problems, where long and short term dependencies in time series can be solved stably. The key parameter of LSTM networks is the memory cell, which remembers the past time state. LSTM networks can add or remove information to the cell state through three control gates (input gate, forget gate, and output gate) The overall architecture is shown in Fig. 5. The computational process of the LSTM is described as follows.

(1) When new input arrives, the input information can be accumulated if and when the input gate is activated.

(2) If the forget gate is activated, past cell states can be ignored in that cell.

(3) The output gate can control the latest unit output can be propagated to the final state.

In the current flow prediction, $x = (x_1, x_2, \ldots\ldots, x_T)$ is the historical input data and $y = (y_1, y_2, \ldots\ldots, y_T)$ is the predicted data. The preset flow rate can be calculated as:

$$i_t = \sigma(W_{ix}x_t + W_{im}m_{t-1} + W_{ic}c_{t-1} + b_i) \tag{17}$$

$$f_t = \sigma(W_{fx}x_t + W_{fm}m_{t-1} + W_{fc}c_{t-1} + b_f) \tag{18}$$

$$c_t = f_t^{\circ}c_{t-1} + i_t^{\circ}g(W_{cx}x_t + W_{cm}m_{t-1} + b_c) \tag{19}$$

$$o_t = \sigma(W_{ox}x_t + W_{om}m_{t-1} + W_{oc}c_t + b_o) \tag{20}$$

$$m_t = o_t^{\circ}h(c_t) \tag{21}$$

$$y_t = W_{ym}m_t + b_y \tag{22}$$

where i_t denotes input gates, f_t denotes forgetting gates, c_t denotes activation vectors for each cell, o_t denotes output gates, m_t denotes activation vectors for each memory block, W denotes the weight matrix, b denotes the deviation vector and o denotes the scalar product.

$\sigma(\cdot)$ is a standard logic function.

$$\sigma(x) = \frac{1}{1 + e^{-x}} \tag{23}$$

$g(\cdot)$ is the central logical function.

$$g(x) = \frac{4}{1 + e^{-x}} - 2x \in [-2, 2] \tag{24}$$

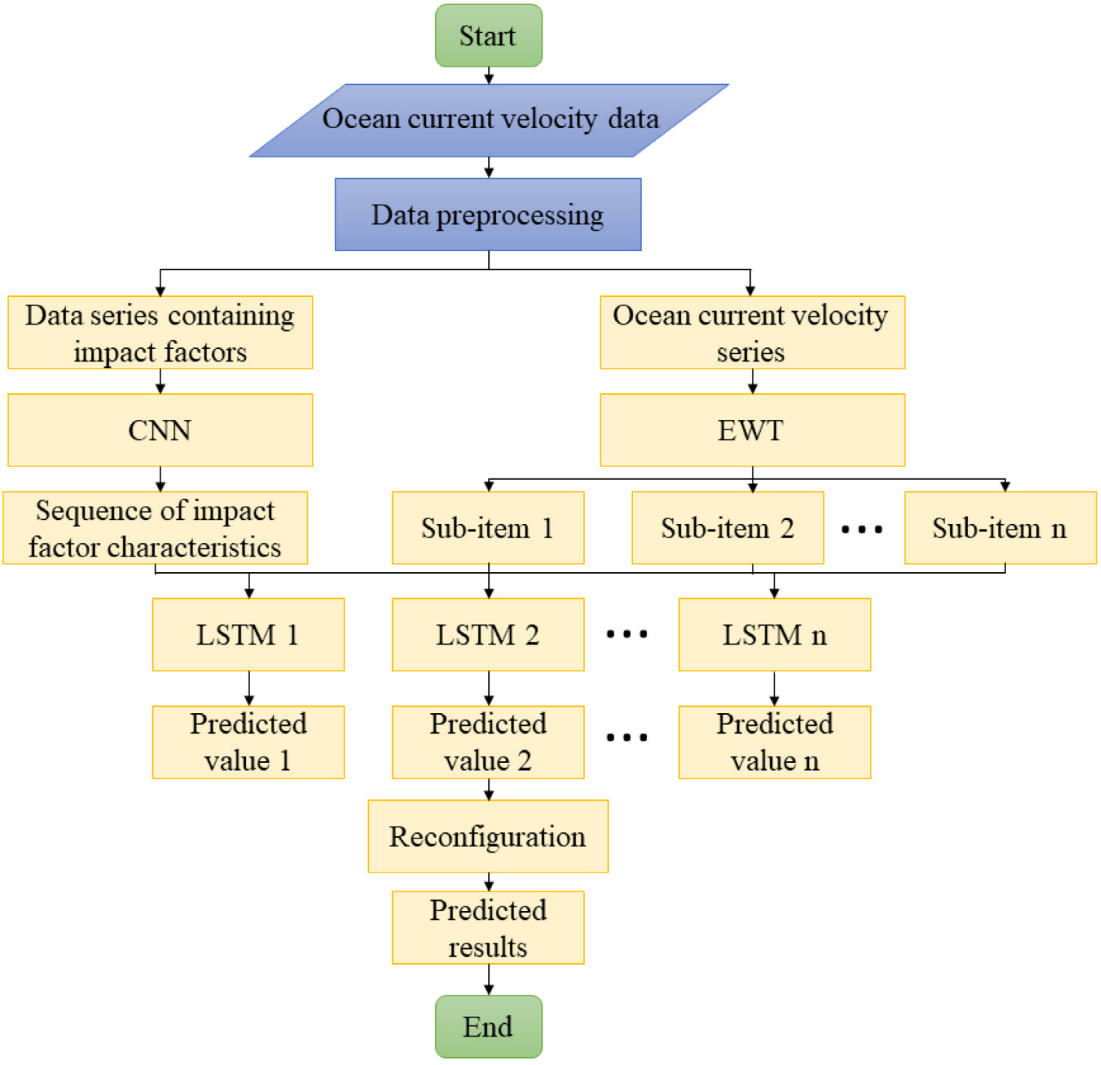

Fig. 4. Flow chart of EWT-LSTM-CNN based prediction model.

```
Model: "sequential_2"
_________________________________________________________________
Layer (type)                 Output Shape              Param #
=================================================================
lstm_4 (LSTM)                (None, None, 32)          4864
_________________________________________________________________
lstm_5 (LSTM)                (None, 64)                24832
_________________________________________________________________
dense_6 (Dense)              (None, 32)                2080
_________________________________________________________________
dense_7 (Dense)              (None, 16)                528
_________________________________________________________________
dense_8 (Dense)              (None, 1)                 17
=================================================================
Total params: 32,321
Trainable params: 32,321
```

Fig. 5. Overall architecture of the network based on LSTM neural networks.

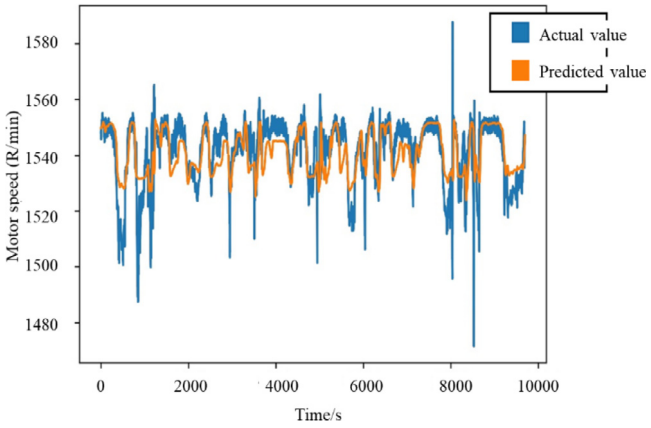

Fig. 6. Predicted and actual pump speed values based on LSTM neural networks. (For interpretation of the references to color in this figure legend, the reader is referred to the web version of this article.)

$h(\cdot)$ is the central logical function.

$$h(x) = \frac{2}{1+e^{-x}} - 2x \in [-1, 1] \tag{25}$$

The test set was selected and pump speed predictions were made, as shown in Fig. 6. Where the actual values are in blue and the predicted values are in orange. The average absolute error between the predicted and actual values is 6.05 r/min. The time cost of a single prediction is 0.001 s. The root mean square error is 2144.92.

3.2. Predictive models based on CNN convolutional layers

The 1D-CNN one-dimensional convolutional neural network is also widely used in time series prediction problems and its main

```
Model: "sequential_1"
_________________________________________________________________
Layer (type)                 Output Shape              Param #
=================================================================
conv1d_3 (Conv1D)            (None, None, 32)          832
_________________________________________________________________
max_pooling1d_2 (MaxPooling1 (None, None, 32)          0
_________________________________________________________________
conv1d_4 (Conv1D)            (None, None, 32)          5152
_________________________________________________________________
max_pooling1d_3 (MaxPooling1 (None, None, 32)          0
_________________________________________________________________
conv1d_5 (Conv1D)            (None, None, 32)          5152
_________________________________________________________________
global_max_pooling1d_1 (Glob (None, 32)                0
_________________________________________________________________
dense_1 (Dense)              (None, 1)                 33
=================================================================
Total params: 11,169
Trainable params: 11,169
```

Fig. 7. Overall architecture of a 1D-CNN neural network based network.

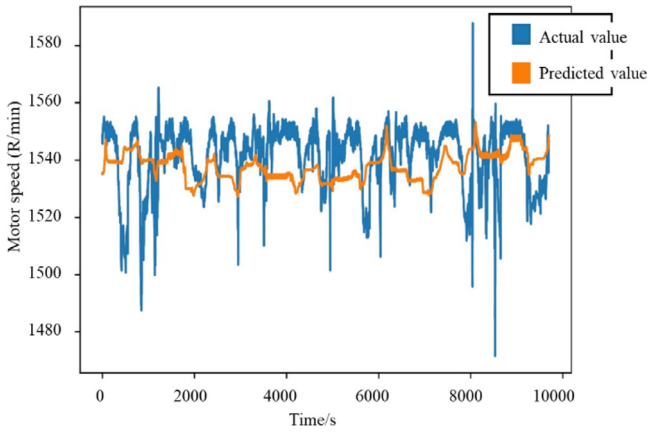

Fig. 8. Predicted and actual values of pump speed based on 1D-CNN neural network. (For interpretation of the references to color in this figure legend, the reader is referred to the web version of this article.)

feature is its relatively low time cost. In order to take into account information from previous temporal data, the inputs are set to data from a past period. If there is more than one input data, the input vectors will be superimposed in the channel direction. $C^{(k-1)}$ is the number of channels in the kth convolution layer and H is the size of the filter. The activation function is ReLU. Thus, the convolution process for the ith filter is expressed as

$$h_{ij}^{(k)} = \phi\Big(\sum_{p=1}^{c^{(k-1)}} \omega \sum_{q=1}^{H} w_{ipq}^{(k)} x_{p,j+q}^{(k)} + b_i^{(k)}\Big) \tag{26}$$

where $w_{ipq}^{(k)}$ is the filter weights, $b_i^{(k)}$ is the filter bias. $x_{p,j+q}^{(k)}$ is the inputs to the layer. The number of filters in each layer is 16, 32 and 64, and H is set to 3. A sliding filter with a stride width of 1 is set to perform the convolution operation. After three convolution layers, the created feature map is fed to the fully connected output layer. The loss function here is the squared error.

Based on the above parameters, the following one-dimensional convolutional neural network was designed by training the pump speed and sensor information under feedforward control, where the overall architecture of the network and the number of neural unit nodes are shown in Fig. 7.

The pump speed prediction by taking the test set is shown in Fig. 8, where the actual values are in blue and the predicted values are in orange. The average absolute error between the predicted and actual values is 10.49 r/min. The time cost of a single prediction is 0.0029 s. The root mean square error is 2086.41. The prediction accuracy is reduced compared to the LSTM neural network, but the time cost of a single prediction is reduced.

3.3. Predictive models based on EWT-LSTM-CNN

In order to combine the advantages of accurate LSTM neural network prediction and low time cost of 1D-CNN, this paper studies the construction of a model based on the combination of EWT-LSTM-CNN. The whole framework of this paper, which combines the advantages of all three, is shown in Fig. 9. It is further described in this paper as follows.

(1) EWT was used to decompose the raw wind speed data into several sub-layers.

(2) The LSTM network was used to predict the high-frequency sub-layers, while the 1D-CNN neural network was used to predict the low-frequency sub-layers.

(3) To quantify the superior performance of the EWT-LSTM-CNN prediction model, several models were taken for comparison. The models compared include the fully connected model, the LSTM model and the CNN model.

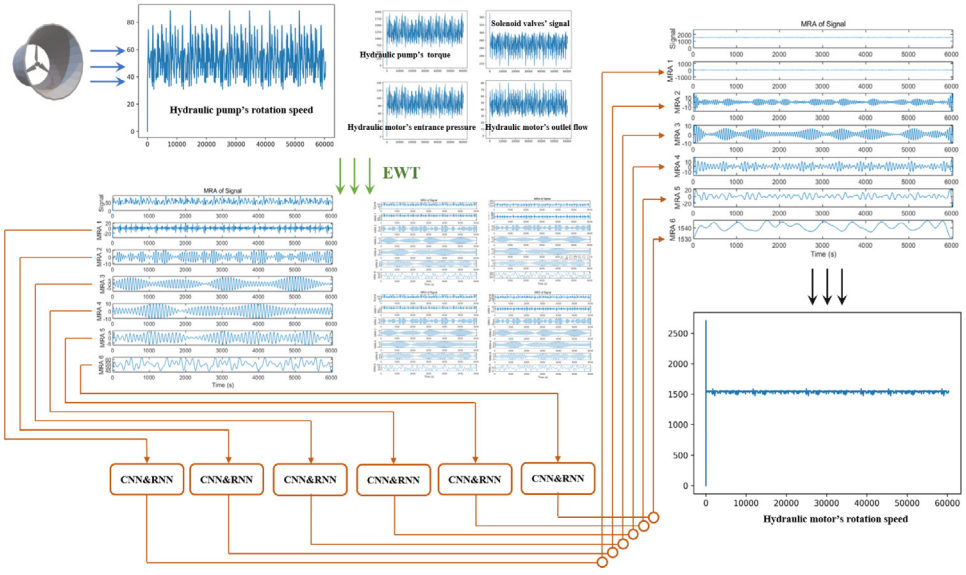

Fig. 9. Overall framework of EWT-LSTM-CNN prediction model.

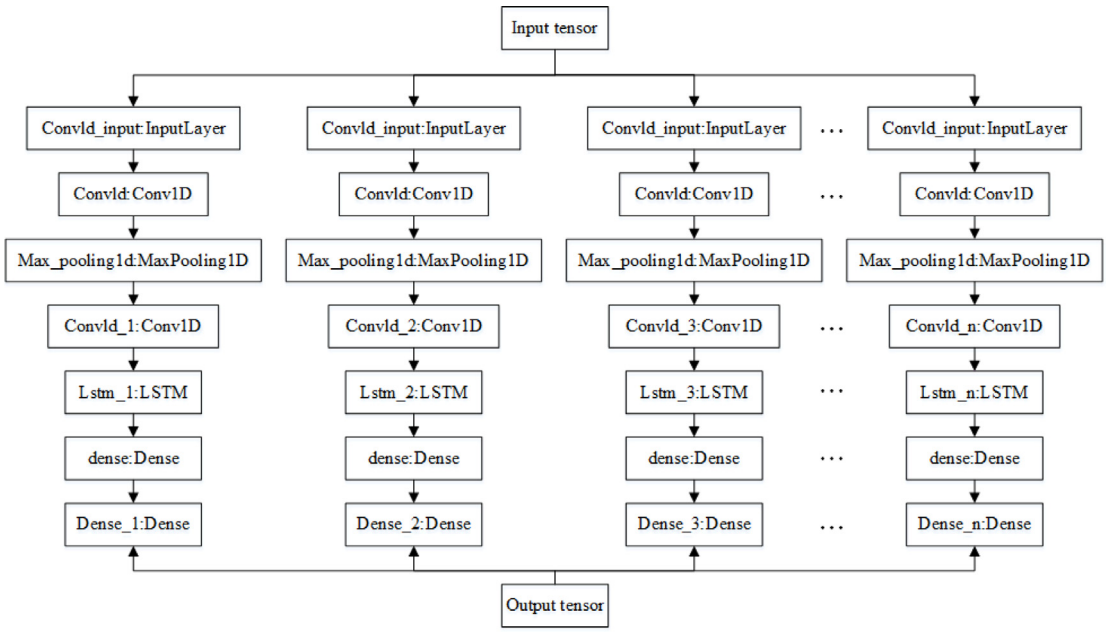

Fig. 10. The overall framework of EWT-LSTM-CNN based neural network.

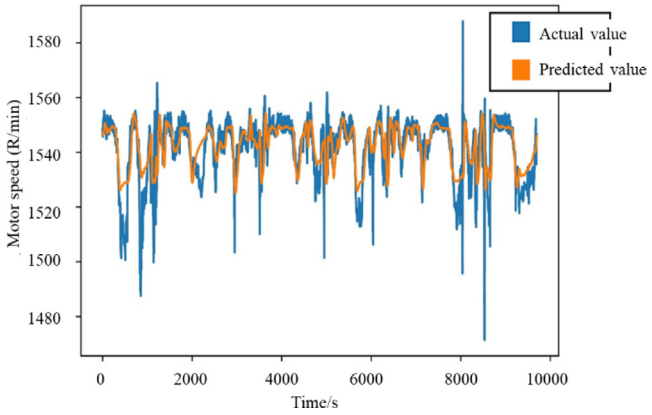

Fig. 11. Predicted and actual values of motor speed based on EWT-LSTM-CNN prediction model. (For interpretation of the references to color in this figure legend, the reader is referred to the web version of this article.)

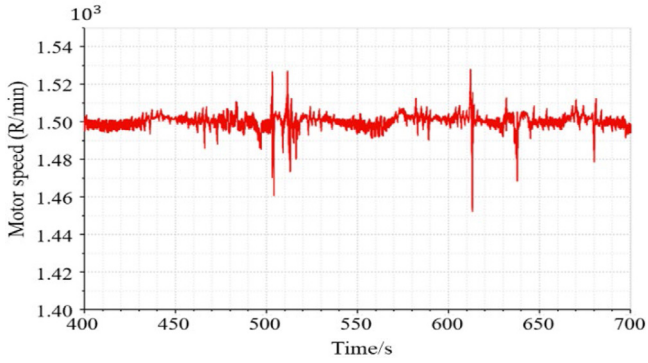

Fig. 12. Motor speed profile based on a deep learning predictive model.

An EWT can be defined as a set of band-pass filters selected according to the spectral characteristics of a signal. In order to determine the frequency range of the band pass filters, the Fourier spectrum of the signal is segmented and the EWT can effectively identify and extract a finite number of intrinsic modes of a system.

For flow time series, the main steps of the EWT algorithm are (1) expanding the signal, (2) performing the Fourier transform form, (3) extracting the boundaries, (4) constructing the filter bank, and (5) extracting the sub-bands.

The information from the pump speed and sensors under feedforward control is trained and the following EWT-LSTM-CNN neural network is designed in this paper. The overall architecture of the network is shown in Fig. 10.

The pump speed predictions are shown in Fig. 11, where the actual values are in blue and the predicted values are in orange. The average absolute error between the predicted and actual values is 5.31 r/min. The time cost of a single prediction is 0.046 s. The root mean square error is 1955.30. Compared to the commonly used short-term memory neural network, the prediction accuracy is improved by 12.26% and the time cost of a single prediction is also less than the sampling time of the constant frequency control algorithm.

4. AMESim and simulik simulation of hydraulic transmission and control power generation equipment system

4.1. Joint simulation based on AMESim and simulink

A deep learning predictive model based on EWT-LSTM-CNN is introduced in AMESim and Simulink, and a compensated controller is implemented. The above control algorithm allows the variation of pump speed in a hydraulic transmission control system to be obtained. In this paper, the dynamic accuracy is calculated by taking the variation of pump speed from 400–700 s, and the dynamic accuracy is compared with the traditional constant frequency control algorithm as shown in Fig. 12.

In summary, the dynamic accuracy of the motor speed with the deep learning predictive model-based constant frequency control algorithm is 0.3%, which is a 90% improvement compared to the dynamic accuracy of the motor speed with the feed-forward PID control algorithm.

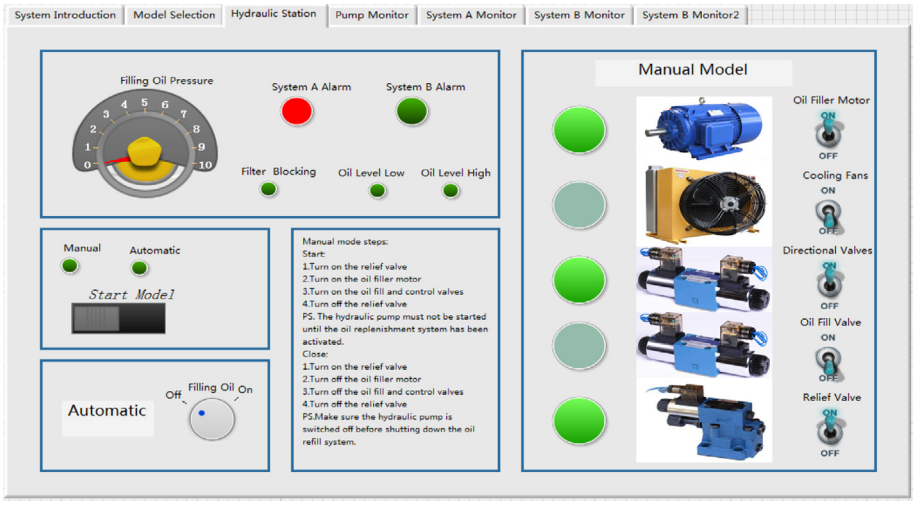

Fig. 13. Operating interface of the hydroelectric power generation system for ocean currents.

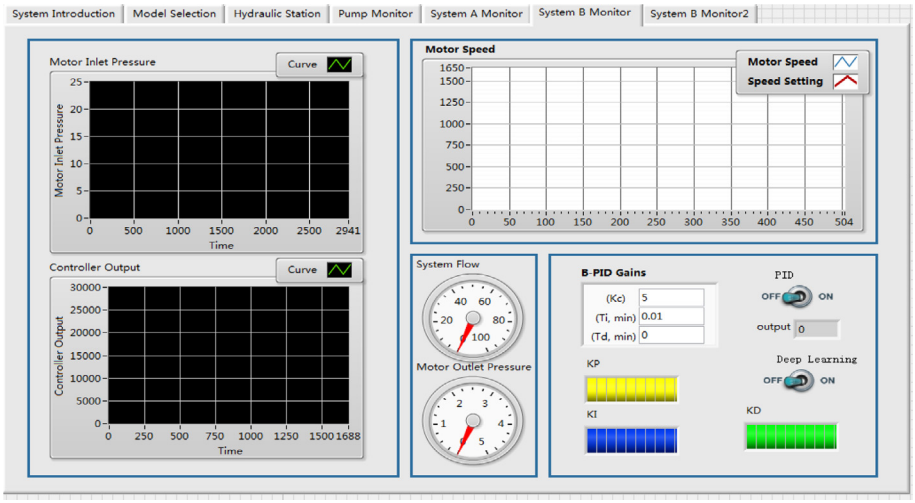

Fig. 14. Status monitoring interface for hydroelectric power generation systems.

4.2. Control system design for deep learning constant frequency control

The main functions of the control system of the hydraulic transmission and control power generation equipment are implemented in two main ways: automatic mode and manual mode. This is shown in Fig. 13.

The main functions implemented in this system include simulation of speed, oil replenishment, system unloading, cooling oil circuit control, constant speed control, and operating status monitoring (pump speed, motor speed, pump outlet pressure, motor inlet pressure, system flow), as shown in Fig. 14. The project uses a three-tier control system, with Programmable Logic Controller PLC1 and PLC2 controlling each of the three hardware systems of the hydraulic transmission and control power generation equipment.

The communicates with the Inter-Process Communication (IPC) via Transmission Control Protocol/Internet Protocol (TCP/IP) protocol to obtain the sensor parameters of the hydraulic system and visualize the data in real time. In addition, this paper focuses on running some deep learning prediction models. The more computationally intensive calculations in the constant frequency control algorithm are sent to the IPC side, which in turn calls its Application Programming Interface (API) on the PLC to achieve high precision constant frequency control, as shown in Fig. 15. The PC side integrates the following functions: project construction, network communication connection, data acquisition, data processing, training of deep learning prediction models and constant frequency control. In order to efficiently and stably implement these functions as above, this paper designs the control software on the PC side based on a multi-process approach.

5. Experimental study of hydraulic constant frequency control algorithms

5.1. Test equipment

The hydraulic transmission and power generation test bench is used to carry out experimental research on constant frequency control algorithms. The system power of this test bench is 50 kW and the whole test bench consists of three main parts: the speed simulation system, the hydraulic transmission and control power generation system, and the cooling, and oil change system. This is shown in Fig. 16.

The main technical parameters of hydraulic transmission and power generation test bench are shown in Table 1, which is arranged in a 2-tow-2 distributed configuration.

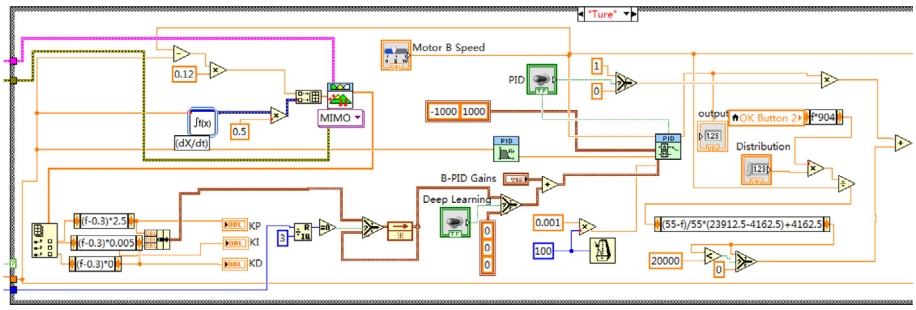

Fig. 15. Block diagram of the main control algorithm of the system.

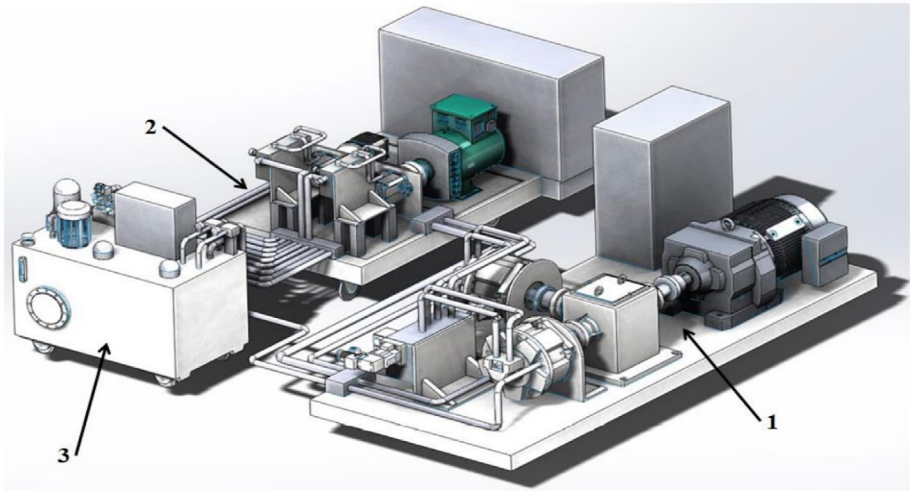

Fig. 16. Hydraulic power transmission and control test bench. 1-speed simulation system. 2-hydraulic transmission and control of power generation system. 3-hydraulic cooling oil change system.

Through the speed simulation system, combined with Simulink simulation of the turbine output characteristics, this paper can simulate the speed variation of the turbine under the change of ocean current flow velocity through the inverter and motor. The core components of this include inverter, motor, reducer, and coupling, as shown in Fig. 17.

The core components of the hydraulically controlled power generation system, shown in Fig. 18, include components such as dosing pumps, variable motors, valve blocks, proportional amplifiers and hydraulic oil circuits. When the turbine speed variation is simulated by the speed simulation system, the hydraulic transmission and control system is used to keep the generator speed and the variable motor speed constant (generator and variable motor are rigidly connected) to achieve high quality power generation.

5.2. Experimental data acquisition

In order to conduct an experimental study of a constant frequency control algorithm for deep learning predictive models, experimental data is first collected and a training set is constructed. The training set is used to train the deep learning model. The network communication module and the data acquisition module are run to collect the values of each sensor within the hydraulic system. As PC software development is based on a multi-process approach, there is a separate memory space and environment space between multiple processes. In order to visualize the collected data in the interface processes, inter-process communication techniques are used. In contrast to other inter-process communication methods, shared memory can be read and written directly to memory and does not require any data copying. The data acquisition module communicates with the PLC via the ModBus protocol and the PC side communicates with the IPC via the TCP/IP protocol. The IPC and PC side are based on Labview and Python for network communication respectively.

Table 1
Technical parameter of the ocean current energy hydraulic transmission and control power generation system.

Technical parameter	Parameter value
Hydraulic system pressure (MPa)	21
Hydraulic pump speed range (r/min)	30∼100
Setting value for hydraulic motor speed (r/min)	1500
Safety valve pressure (MPa)	30
Refill oil system pressure (MPa)	4
Controlling oil pressure (MPa)	3
Hydraulic system flow (l/min)	0∼180
Refill oil system flow rate (l/min)	30

The hydraulic pump speed and motor speed over a 100 min period, as shown in Fig. 19(a) and (b), show the speed status of the power and actuator components of the hydraulic system. The output pressure of the hydraulic pump and the input pressure of the hydraulic motor over a period of 100 min reflect the pressure state of the hydraulic system as shown in Fig. 19(c) and 19 (d). The hydraulic motor displacement variation curve and the hydraulic system flow rate curve over a 100 min period reflects the system flow rate variation as shown in Fig. 19(e) and (f).

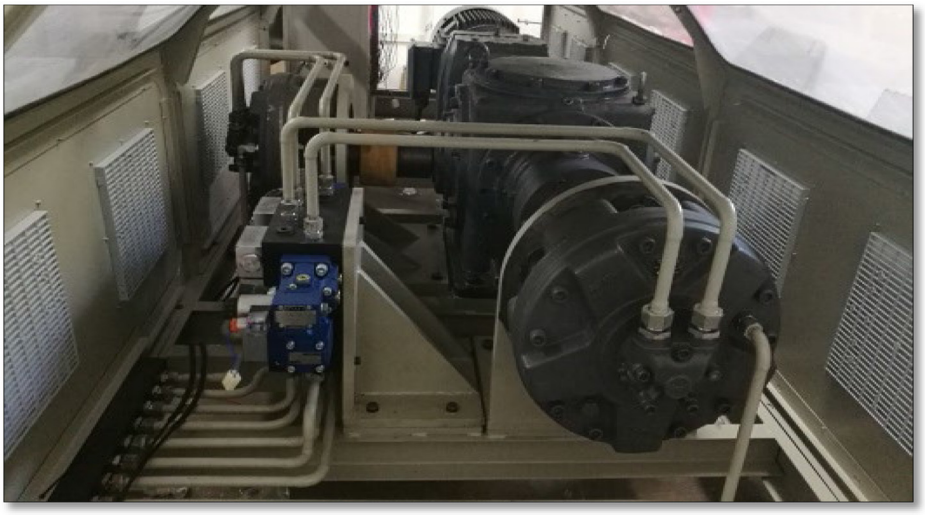

Fig. 17. Turbine speed simulation system.

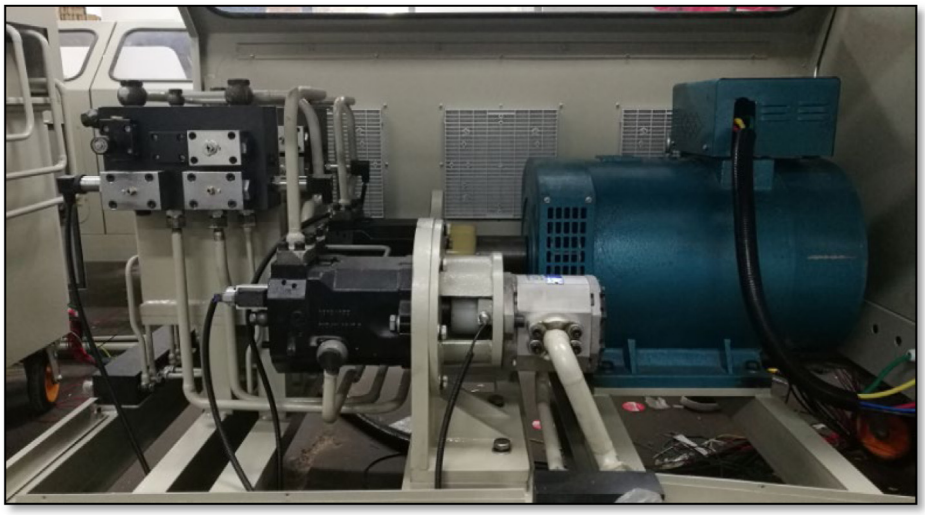

Fig. 18. Hydraulic energy transfer power generation system.

5.3. Experimental results

The data processing and model training modules were run to train and tune the sensor signals to obtain a deep learning prediction model suitable for this bench, the experimental process is shown in Fig. 20.

Experiments with feedforward control algorithms, feedforward PID control algorithms and control algorithms based on deep learning predictive models for constant frequency control were run separately, and the motor speed under these algorithm conditions for the 400 s–1000 s time period is shown in Figs. 21–23.

The constant frequency control algorithm based on the deep learning EWT-LSTM-CNN predictive model for the 400–1000 s time period on the motor speed has an average value of 1500.17 and an STD standard deviation of 7.73, which improves the STD standard deviation index by 78.11% compared to the feed-forward PID algorithm. The simulation study of the algorithm verifies that the constant frequency control algorithm based on the EWT-LSTM-CNN prediction model can effectively improve the dynamic accuracy of the constant frequency of the motor of the hydraulic transmission control power generation equipment and thus improve the quality of the system power generation.

6. Discussion

In this paper, some parameters in the constant-frequency control algorithm based on a deep learning prediction model are adjusted and further tuned and optimized for the experimental bench. The research content of this paper realizes efficient absorption and conversion technology of unsteady ocean current energy to achieve continuous and efficient power generation and high-quality power generation, solving the problem of self-sufficiency of underwater sensor power and meeting the power supply needs of underwater observation platforms and other equipment in some sea areas. At the same time, it can also provide stable electricity for remote islands. Due to the limitation of the controller's arithmetic power, it is not possible to improve the constant frequency dynamic accuracy by shortening its sampling time, and it is not possible to run a deep learning prediction model with better prediction results on it. If these two problems can be solved effectively, the control effect will be further improved.

7. Conclusion

Hydraulic transmission-controlled power generation systems drive synchronous generator rotation directly through hydraulic

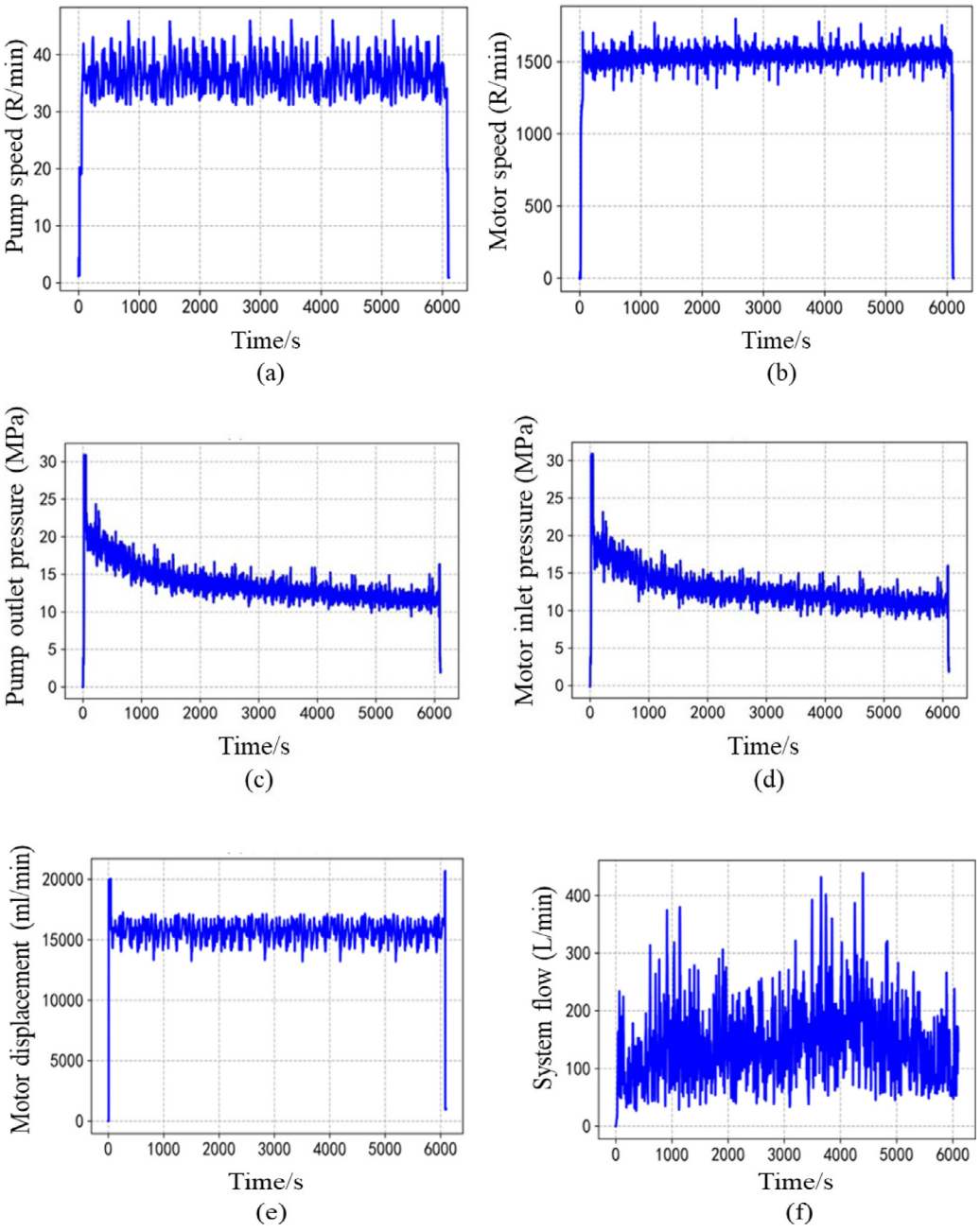

Fig. 19. Acquisition of the values of the parameters of the hydraulic transmission and control test bench.

Fig. 20. Experimental procedure for model training.

motors, and the accuracy of the hydraulic motor speed determines the generator generation frequency (i.e. the quality of power generation). In this paper, the quality of power generation is achieved through a deep learning algorithm, which realizes accurate control of the hydraulic motor at a constant speed under non-stationary strongly coupled excitation in multiple dimensions such as turbine speed and motor load torque.

(1) This paper analyzes the mathematical model of the hydraulic transmission and control system and proposes a constant frequency control algorithm based on a deep learning EWT-LSTM-CNN prediction model to further improve the dynamic accuracy of the motor speed.

(2) According to the 50 kw hydraulic transmission and control power generation equipment, a joint simulation platform based on AMESim and Simulink is constructed in this paper.

(3) The deep learning prediction model of EWT-LSTM-CNN constructed in this paper improved the prediction accuracy by 12.26% compared to the commonly used short-term memory neural networks. Moreover, the time cost of a single prediction is

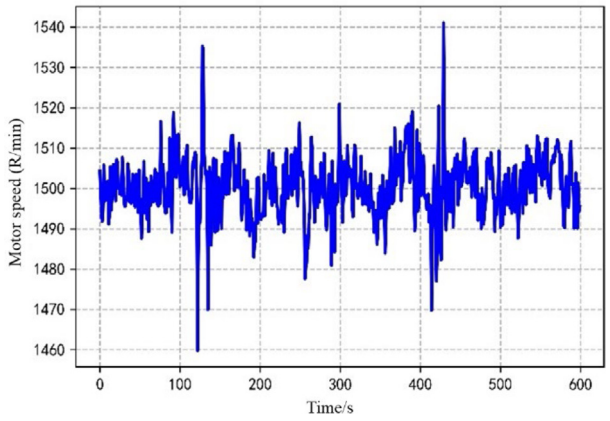

Fig. 21. Motor speed profile based on feed-forward control algorithm.

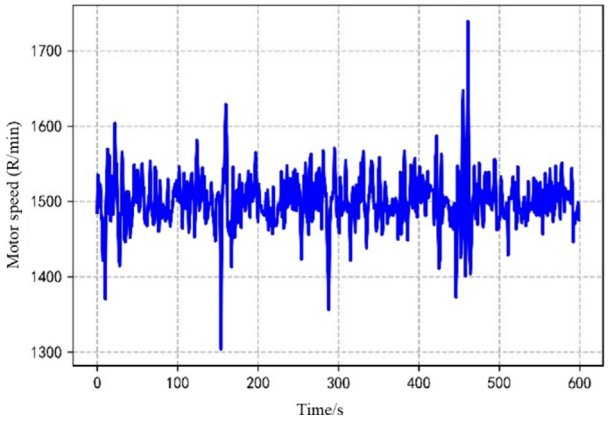

Fig. 22. Motor speed profile based on feed-forward PID control algorithm.

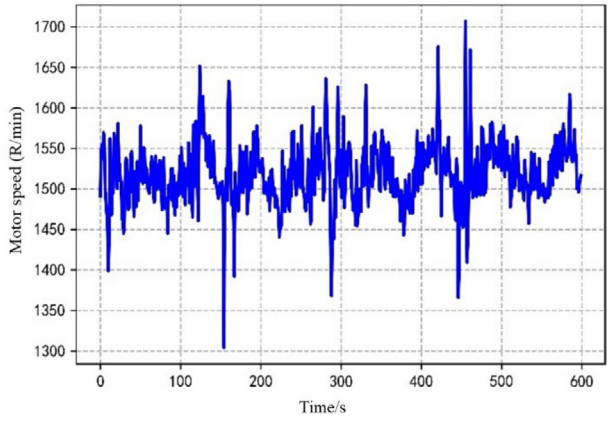

Fig. 23. Motor speed profile under EWT-LSTM-CNN predictive model based constant frequency control algorithm.

smaller than the sampling time of the constant frequency control algorithm.

(4) By simulating the constant frequency control algorithm through the simulation model, the dynamic accuracy of the motor speed under the constant frequency control algorithm based on the deep learning prediction model in this paper is 0.3%, which is 90% better than the dynamic accuracy of the motor speed under the feed-forward PID control algorithm, and can effectively improve the quality of the system's power generation.

(5) This paper investigates the deep learning constant frequency control algorithm using a 50 kW hydraulic transmission control test bench. The maximum deviation of the motor speed based on the deep learning predictive model is 34.17 and the STD standard deviation is 7.73 in the time period of 400–1000 s. Compared with the feed-forward PID algorithm, the STD standard deviation index of the deep learning algorithm is improved by 78.11% and the maximum deviation is reduced by 86.10%. This paper validates the simulation study of the algorithm, and the constant frequency control algorithm based on the deep learning prediction model can effectively improve the dynamic accuracy of the constant frequency of the motor of the hydraulic transmission control power generation equipment, and then improve the quality of the system power generation.

CRediT authorship contribution statement

Hongbo Wei: Conceptualization, Methodology, Writing–original draft, Validation. **Wenbin Su:** Data curation. **Junxiao Shi:** Software.

Declaration of competing interest

The authors declare that they have no known competing financial interests or personal relationships that could have appeared to influence the work reported in this paper.

Data availability

No data was used for the research described in the article.

Acknowledgment

This project was supported by the equipment pre-research and sharing technology project of the equipment development department of China Military Commission (No. 41421080302).

References

Djama Dirieh, N., Thiébot, J., Guillou, S., Guillou, N., 2022. Blockage corrections for tidal turbines—Application to an array of turbines in the alderney race. Energies 15, 3475. http://dx.doi.org/10.3390/en15103475.

Hazim, S., El Ouatouati, A., Taha Janan, M., Ghennioui, A., 2020. Performance of a hydrokinetic turbine using a theoretical approach. Energy Rep. 6, 317–324. http://dx.doi.org/10.1016/j.egyr.2019.08.062.

Jacobs, G., D'Addezio, J.M., Ngodock, H., Souopgui, I., 2021. Observation and model resolution implications to ocean prediction. Ocean Model. 159, 101760. http://dx.doi.org/10.1016/j.ocemod.2021.101760.

Jiang, C., Shu, X., Chen, J., Bao, L., Xu, Y., 2021. Research on blade design of lift–drag-composite tidal-energy turbine at low flow velocity. Energies 14, 4258. http://dx.doi.org/10.3390/en14144258.

Kim, G., Lee, M.E., Lee, K.S., Park, J.-S., Jeong, W.M., Kang, S.K., Soh, J.-G., Kim, H., 2012. An overview of ocean renewable en-ergy resources in Korea. Renew. Sustain. Energy Rev. 16, 2278–2288. http://dx.doi.org/10.1016/j.rser.2012.01.040.

Li, M., Luo, H., Zhou, S., Senthil Kumar, G.M., Guo, X., Law, T.C., Cao, S., 2022a. State-of-the-art review of the flexibility and fea-sibility of emerging offshore and coastal ocean energy technologies in East and Southeast Asia. Renew. Sustain.-Ble Energy Rev. 162, 112404. http://dx.doi.org/10.1016/j.rser.2022.112404.

Li, Y., Ma, X., Tang, T., Zha, F., Chen, Z., Liu, H., Sun, L., 2022b. High-efficient built-in wave energy harvesting technology: From laboratory to open ocean test. Appl. Energy 322, 119498. http://dx.doi.org/10.1016/j.apenergy.2022.119498.

Liu, J., Yang, J., Liu, K., Xu, L., 2022. Ocean current prediction using the weighted pure attention mechanism. Jmse 10, 592. http://dx.doi.org/10.3390/jmse10050592.

Nachtane, M., Tarfaoui, M., Goda, I., Rouway, M., 2020a. A review on the technologies, design considerations and numerical models of tidal current turbines. Renew. Energy 157, 1274–1288. http://dx.doi.org/10.1016/j.renene.2020.04.155.

Nachtane, M., Tarfaoui, M., Goda, I., Rouway, M., 2020b. A review on the technologies, design considerations and numerical models of tidal current turbines. Renew. Energy 157, 1274–1288. http://dx.doi.org/10.1016/j.renene.2020.04.155.

Nasr Esfahani, F., Darwish, A., Williams, B.W., 2022. Power converter topologies for grid-tied solar photovoltaic (PV) powered electric vehicles (EVs)—A comprehensive review. Energies 15, 4648. http://dx.doi.org/10.3390/en15134648.

Qadir, S.A., Al-Motairi, H., Tahir, F., Al-Fagih, L., 2021. Incentives and strategies for financing the renewable energy transition: A review. Energy Rep. 7, 3590–3606. http://dx.doi.org/10.1016/j.egyr.2021.06.041.

Su, W., Wei, H., Guo, P., Hu, Q., Guo, M., Zhou, Y., Zhang, D., Lei, Z., Wang, C., 2021. Research on hydraulic conversion technology of small ocean current turbines for low-flow current energy generation. Energies 14, 6499. http://dx.doi.org/10.3390/en14206499.

Wang, J., Chen, Z., Zhang, F., 2021. A review of the optimization design and control for ocean wave power generation systems. Energies 15, 102. http://dx.doi.org/10.3390/en15010102.

Zhang, H., Chen, H.H., Lao, K., Ren, Z., 2022. The impacts of resource endowment, and environmental regulations on sustaina-bility—Empirical evidence based on data from renewable energy enterprises. Energies 15, 4678. http://dx.doi.org/10.3390/en15134678.

Zhang, D., Ma, X., Si, Y., Huang, C., Huang, B., Li, W., 2017. Effect of doubly fed induction GeneratorTidal current turbines on stability of a distribution grid under unbalanced voltage conditions. Energies 10, 212. http://dx.doi.org/10.3390/en10020212.